RESEARCH ARTICLE

ADVANCED OPTICAL MATERIALS
www.advopticalmat.de

Thermal/Water-Stable $CsPbX_3@SiO_x$ Core–Shell Quantum Dots for Inkjet Printing and Potential Color Converting Applications

Seong Yeon Park, Gayoung Seo, Taeyeon Kim, Carina Pareja-Rivera, Fabian Pino, YoonGyo Kim, Jorge Simancas, Byeongsung Kim, Ignacio Utreras-Asenjo, Jhonatan Rodriguez-Pereira, Hyeonyeong Jo, JaeHong Park, Jin Ho Bang, Sofia Masi, Seog Joon Yoon, Iván Mora-Seró,* and Andrés F. Gualdrón-Reyes**

Ligand-mediated surface passivation is widely used to fill defect sites and stabilize perovskite nanoparticles, keeping their photophysical properties unchanged. However, this strategy can promote the growth of agglomerates, quenching the luminescence of nanoparticles. Additionally, the presence of bulky ligands can hinder the interparticle carrier transport, difficulting the fabrication of efficient optoelectronic devices. In this work, the synthesis of SiO_x-covered $CsPbX_3$ PQDs ($CsPbX_3@SiO_x$) is performed through a modified ligand-assisted reprecipitation method (LARP), by adding 3-aminopropyl-triethoxysilane (APTES) and oleic acid to the mixture reaction. Here, it is possible to suppress the aggregates formation, achieving water-stable single core–shell PQDs with a photoluminescence quantum yield of up to 99.4% and facile bandgap modulation by varying the halide content. Accordingly, $CsPbX_3@SiO_x$ PQDs inks are obtained for preparing inkjet-printed QR codes and color converters, with stable luminescence up to 1.5 and 9 h of continuous operation at 2.5 V for Cl/Br- and Br-perovskites, respectively. Interestingly, a PL splitting is observed for the Br/I-perovskite along the time, indicating the emergence of halide migration to generate Br- and I-rich domains, mediating the generation of white color emission. This contribution offers a prominent alternative to producing single PQDs with suitable optical properties and stability for developing promising LED technologies.

1. Introduction

Lead halide perovskite quantum dots (PQDs) materials have shown immense potential in the field of optoelectronics and photovoltaics, such as light-emitting diodes (LEDs),[1–4] solar cells,[5–7] lasers[8] and biomedical devices,[9,10] owing to their outstanding optical and electronic properties. Particularly, 3D cesium lead halide ($CsPbX_3$, X = Cl, Br, I) PQDs exhibit a large absorption coefficient,[11] high photoluminescence quantum yields (PLQYs),[12,13] tunable bandgap,[14] and exceptional charge carrier dynamics.[15,16] However, despite their unique optoelectronic properties, their practical application is often hindered by main challenges related to poor structural stability, the appearance of surface defects, and photo-oxidative degradation.[17,18] One of the primary challenges is the intrinsic instability of $CsPbX_3$ PQDs. Although the nanoconfinement feature in PQDs is ideal for avoiding the octahedra tilting observed in bulk materials,[19] these

S. Y. Park, G. Seo, T. Kim, Y. Kim, B. Kim, H. Jo, S. J. Yoon
Department of Chemistry
College of Natural Science
Yeungnam University
Gyeongsan 38541, Republic of Korea
E-mail: yoon@yu.ac.kr

The ORCID identification number(s) for the author(s) of this article can be found under https://doi.org/10.1002/adom.202500968

DOI: 10.1002/adom.202500968

S. Y. Park, G. Seo, T. Kim, C. Pareja-Rivera, F. Pino, J. Simancas, S. Masi, I. Mora-Seró, A. F. Gualdrón-Reyes
Institute of Advanced Materials (INAM)
Universitat Jaume I (UJI)
Avenida de Vicent Sos Baynat, s/n, Castellón de la Plana, Castellón 12071, Spain
E-mail: sero@uji.es; gualdron@uji.es, andres.gualdron@uach.cl

I. Utreras-Asenjo, A. F. Gualdrón-Reyes
Facultad de Ciencias
Instituto de Ciencias Químicas
Universidad Austral de Chile
Isla Teja, Valdivia 5090000, Chile

J. Rodriguez-Pereira
Center of Materials and Nanotechnologies
Faculty of Chemical Technology
University of Pardubice
Nam. Cs. Legii 565, Pardubice 53002, Czech Republic

materials can be susceptible to decompose or degrade under external stimuli such as moisture, oxygen, heat, applied bias, and ultraviolet (UV) light.[16,20] This degradation is often accompanied by the formation of non-radiative recombination centers, which quench the photoluminescence (PL) and reduce the efficiency of devices. To address these challenges, several strategies have been constantly proposed to improve the extrinsic and intrinsic structural stabilities of PQDs; ligand modification,[21–23] core–shell structure,[24] crosslinking,[25] and metal doping.[26]

In this context, recent research has demonstrated significant progress in the field of shell encapsulation for PQDs, to improve their stability and optical performance. Among these strategies, core–shell structure involves an interesting strategy to cover the $CsPbX_3$ PQDs with various types of shells. These protective coverages include organic polymers such as polymethyl methacrylate,[27] poly(vinylidene fluoride) (PVDF)[28,29] and polystyrene,[30] inorganic materials such as SiO_2,[31,32] Al_2O_3,[33] and TiO_2,[34] and perovskites such as $CsPbBr_x$, Cs_4PbX_6,[35] $CsPb_2Br_5$,[36] Rb_4PbBr_6[37] to form a core–shell architecture. The use of SiO_x materials as encapsulating shells has shown promising results, especially in providing robust protection against environmental degradation and enhancing the thermal and chemical stability of PQDs.[38–40] Nevertheless, in these encapsulation examples, the resulting products typically contain multiple particles within a single shell, leading to large particle sizes.[41] Generally, $CsPbX_3$ PQDs utilized in optoelectronic devices are assembled as films, where such large particles can detrimentally affect film quality and, consequently, decrease the device's performance.[17]

In this study, $CsPbBr_3@SiO_x$ PQDs were successfully synthesized by the ligand-assisted reprecipitation process (LARP) at the ambient condition of a single-particle level. Here, 3-aminopropyltriethoxysilane (APTES), featuring amino group, plays a crucial role in the surface passivation of PQDs by exploiting the high binding capability of this surface ligand.[42,43] Also, getting advance of our earlier work,[40] to control the hydrophilicity on the surface, a long carbon chain (C18) ligand, oleic acid, was utilized to enhance the dispersity of PQDs in the solvent medium. We show that this passivation strategy enhances the optical properties of PQDs, reduces non-radiative recombination, preserves high PLQY up to 99.4%, and improves stability against water. In this context, it was possible to prepare suitable $CsPbBr_3@SiO_x$ films under annealing treatment, exhibiting high resistance to H_2O molecules and PQDs inks for inkjet printing applications, achieving well-defined QR codes, and the fabrication of color converters by depositing PQDs active layers on commercial LEDs, generating luminescence under continuous operation up to 9 h. Here, blue- and green-LEDs can be obtained with their corresponding PL emission, while red-LED shows a PL splitting during its operation. We deduce the occurrence of interparticle halide migration in the Br/I-perovskite active layer, obtaining Br- and I-rich domains with a progressive PL increase and mediating the generation of white color emission. Our research demonstrates that SiO_x shell encapsulation is a viable strategy for improving thermal/water durability of PQDs, with the possibility to modulate the intrinsic properties through composition engineering to unlock their potential for color-converting applications. This work marks a significant step forward in the practical application of QDs-based materials, potentially revolutionizing the fields of display technology and printed electronics.

2. Results and Discussion

Monodisperse colloidal $CsPbBr_3@SiO_x$ core–shell PQDs were synthesized through the LARP method at ambient conditions, using APTES as the silica source for the SiO_x formation, and main surface ligand considering its amine group. Ethylene glycol (EG) and oleic acid (OA) were used as coordinating ligands during the synthesis. As shown in Figure S1A (Supporting Information) and **Figure 1A**, in situ UV–vis absorption and PL spectroscopy allowed us to monitor the formation process of $CsPbBr_3@SiO_x$ PQDs in real-time. Here, it is possible to note how the absorption and PL intensities increase from 0 s (where the reaction initiates) to reach 0.85 s. In both cases, the absorption edge/PL emission $CsPbBr_3@SiO_x$ PQDs were shifted from 490/498 nm to 495/507 nm, revealing a formation rate constant from PL of 1.15 s^{-1}, see Figure S1B (Supporting Information). This indicates a fast formation dynamic of PQDs through the LARP procedure, in the presence of APTES ligand. Similar to our earlier work, the formation of perovskite core occurred instantaneously.[40] Here, when the PQDs precursor is added into the stirred anti-solvent, as the time-zero, the LARP reaction occurred in ≤1 s (see details in the Experimental Section in Supporting Information), achieving a similar PL peak position to the one obtained at 30 s, see Figure S1C (Supporting Information). However, the reaction time is extended to 30 s with the purpose of avoiding agglomeration and completing the reaction. Then, high-resolution transmission electron microscopy (HRTEM) depicts the core–shell structure of $CsPbBr_3@SiO_x$ PQDs at different spots, see Figure S2A-A″ (Supporting Information). From these images, a total number of 100 nanoparticles were considered, estimating that 89% correspond to SiO_x-covered single PQDs, 7% are associated with SiO_x-covered multiple PQDs and 4% are ascribed to empty SiO_x shells, see Figure S2B (Supporting Information). Moreover, it is visible that the core possesses a well-defined crystalline structure with a characteristic lattice plane distance of ≈ 0.26 nm, corresponding to the *d*-spacing of (200) crystal planes of cubic $CsPbBr_3@SiO_x$ PQDs, see Figure S2C (Supporting Information). The average sizes of

J. Rodriguez-Pereira
Central European Institute of Technology
Brno University of Technology
Purkynova 123, Brno 61200, Czech Republic
J. Park
Department of Chemistry and Nanoscience
Ewha Womans University
Seoul 03760, Republic of Korea
J. H. Bang
Department of Applied Chemistry
Center for Bionano Intelligence Education and Research
Hanyang University ERICA
55 Hanyangdaehak-ro, Sangnok-gu, Ansan, Gyeonggi-do 15588, Republic of Korea
J. H. Bang
Department of Energy and Bio Sciences
Hanyang University ERICA
55 Hanyangdaehak-ro, Sangnok-gu, Ansan, Gyeonggi-do 15588, Republic of Korea

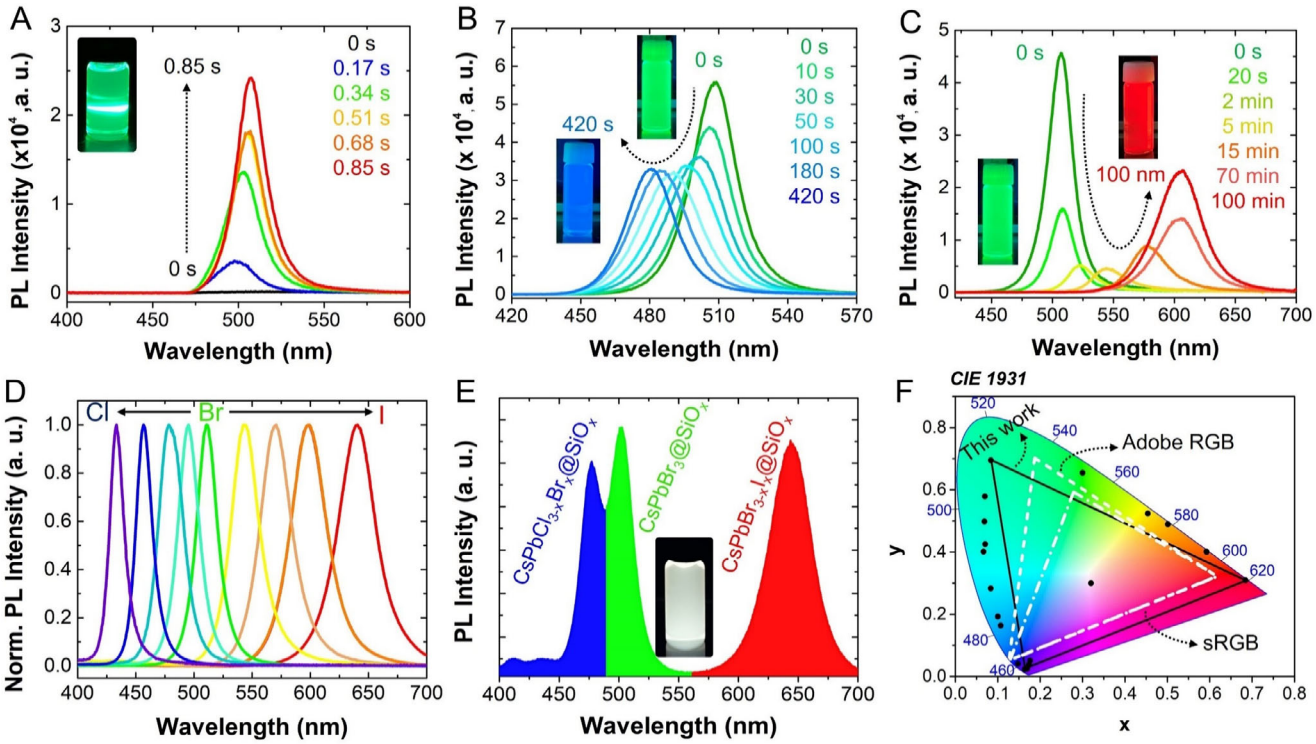

Figure 1. In situ PL measurements showing (A) the formation of green-emitting $CsPbBr_3@SiO_x$ PQDs, and halide exchange process to produce (B) blue-emitting $CsPbCl_{3-x}Br_x@SiO_x$ and (C) $CsPbBr_{3-x}I_x@SiO_x$ PQDs. (D) Normalized PL emission spectra of the tunable composition of $CsPbX_3@SiO_x$ (X═Cl/Br, Br, and Br/I). E) Solution-state white emission spectra obtained by combining the as-prepared $CsPbX_3@SiO_x$. F) CIE chromaticity diagram of as-prepared $CsPbX_3@SiOx$ PQDs, including the color index of the produced white color in (E). The insets of the Figures show the corresponding luminescent photographs of prepared PQD dispersed solutions. Inset in (A) demonstrates the Tyndall effect to prove PQD dispersity in the solution.

$CsPbBr_3$ core and $CsPbBr_3@SiO_x$ estimated from TEM were ≈9.6 ± 1.6 nm and 26.6 ± 4.5 nm, respectively, see Figure S2D,E (Supporting Information). Therefore, the SiO_x shell thickness was determined to be ≈8.5 ± 3.1 nm. To corroborate the existence of single $CsPbBr_3@SiO_x$ PQDs, DLS measurements, see Figure S2F (Supporting Information), and typical SEM images of an active layer prepared from a diluted solution (≈3 μg·mL^{-1}) on Si substrate, see Figure S3A,B (Supporting Information), also demonstrated the formation of nanoparticles with average particle sizes ≈17.6 nm and 17.4 ± 1.4 nm, see Figure S3C (Supporting Information), respectively, in good agreement with the value range obtained from TEM. According to these results, we conclude that our synthetic procedure favors mostly the emergence of SiO_x shells covering single PQDs instead of generating a SiO_x matrix. Cs, Pb, Br, and Si elements are uniformly dispersed as indicated by Energy-dispersive X-ray (EDX) elemental mapping images of representative $CsPbBr_3@SiO_x$ PQDs, see Figure S4 (Supporting Information). This homogeneity in distribution indicates that the PQDs were effectively and evenly encapsulated within the SiO_x shells. By analyzing the optical properties of the as-prepared $CsPbBr_3@SiO_x$ PQDs, we determined the absolute PLQY of the material, achieving 99.4%. This value is an indication of the favored surface passivation provided by APTES ligand, decreasing the density of surface defect sites, and enhancing the radiative channel for carrier recombination. Furthermore, one of the coordinating ligands, OA decreases the defect sites by passivating the ammonium cation anchoring group. Then, as reported previously, the PL peak position of $CsPbBr_3$ PQDs can be modulated by varying the APTES content, causing a blueshift in the optical property, see Figure S5A (Supporting Information). This is associated with the formation of a thicker SiO_x shell, caused by the emergence of more —Si—O—Si— linkages by adding more APTES. The chemical mechanism of SiO_x coverage formation is explained below.

By exploiting the bandgap tunability characteristic of PQDs and brittle SiO_x shell, we aimed to obtain mixed halide PQDs by adding a fixed amount of CsX (X═Cl or I) solution dissolved in polar solvent (with various CsX solution volume ratios, total 1 mL, see SI), into $CsPbBr_3@SiO_x$ PQDs through direct halide exchange, obtaining an immediate color change. In this context, Figure 1B,C shows the in situ PL measurement of the formation of blue-emitting $CsPbCl_{3-x}Br_x@SiO_x$ and red-emitting $CsPbBr_{3-x}I_x@SiO_x$ PQDs, respectively. This fact indicates that halide ions can penetrate beyond the SiO_x shell. As shown in Figure S5B,C (Supporting Information), the kinetic changes in the PL peak position of $CsPbX_3@SiO_x$ PQDs over time were tracked and fitted through single-exponential function, estimating the formation rate of Cl- and I-PQDs. The $CsPbBr_{3-x}I_x@SiO_x$ PQDs were able to form within 100 min with a formation kinetic rate of 1.1 × 10^{-3} s^{-1}. Conversely, $CsPbCl_{3-x}Br_x@SiO_x$ PQDs were able to form within 10 min with a formation kinetic rate of ≈7.1 × 10^{-4} s^{-1}. Attending these halide exchange

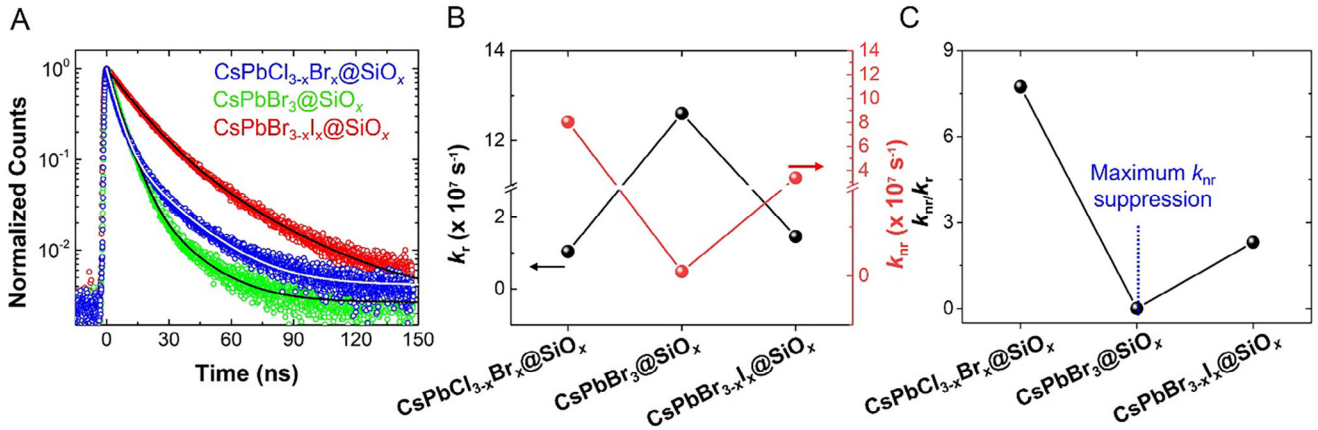

Figure 2. A) Time-resolved PL decay curves, B) radiative (k_r) and non-radiative recombination (k_{nr}) decay constants, and their corresponding C) k_{nr}/k_r ratio for $CsPbX_3@SiO_x$ PQDs colloidal solutions.

rates, it is deductible that the Cl^- incorporation is faster than that of I^- introduction, due to the smaller ionic radius and higher electronegativity of chloride. The PLQY was calculated for $CsPbCl_{3-x}Br_x@SiO_x$ and $CsPbBr_{3-x}I_x@SiO_x$ to be ≈11.5 and 30.2%, respectively. Fourier transform infrared (FTIR) spectra, see Figure S6 (Supporting Information), confirm the formation of $CsPbX_3@SiO_x$ PQDs by the presence of a characteristic peak at 2923 and 2853 cm^{-1} assigned to the stretching vibration of C—H groups from oleic acid and APTES. Additionally, two signals at 1034 and 1116 cm^{-1} from Si—O—C and Si—O—Si vibrations and NH_2 broad stretching band vibration at 3430 cm^{-1} derived from APTES were observed.[40] On the other hand, similar to $CsPbBr_3@SiO_x$ PQDs, TEM images were obtained for $CsPbCl_{3-x}Br_x@SiO_x$ and $CsPbBr_{3-x}I_x@SiO_x$ PQDs, see Figure S7 (Supporting Information), noticing that the nanoparticles are wrapped inside the SiO_x shell. The corresponding particle sizes of mixed Cl/Br- and Br/I-perovskites were 16.4 ± 2.6 nm and 22.8 ± 3.3 nm, respectively. Later, the optical properties of $CsPbX_3@SiO_x$ PQDs colloidal solutions can be precisely tuned across the visible spectrum by modifying the halide composition. Notably, the PL emission peaks exhibit continuous tunability, see Figure 1D, ranging from 433 to 640 nm by controlling the CsX precursor solution volume, 0.3–4 mL, see details in the SI. Taking advantage of the SiO_x shell covering the PQDs, a solution-state white emission was obtained by combining red-, green-, and blue-emissive composite of $CsPbX_3@SiO_x$ samples in an arbitrary ratio, optimally, see Figure 1E. This white light emission is kept for 15 min, after halide exchange produces a single PL emission into the perovskite mixture. Furthermore, the bandgap tunability successfully demonstrated the ability to obtain a multicolor of $CsPbX_3@SiO_x$ PQDs, as evidenced by the CIE chromaticity diagram, covering a more extended area than standard RGB (sRGB) color space (ratio = 166:100) and established adobe RGB (ratio = 123:100), see Figure 1F.

To study the PL recombination dynamics of $CsPbX_3@SiO_x$ PQDs colloidal solutions, time-resolved PL (TRPL) measurements at the maximum PL peak were carried out. As seen in **Figure 2A**, PL decay can be fitted to bi-exponential PL decay, described through the equation: $y = y_0 + A_1e^{-x/\tau_1} + A_2e^{-x/\tau_2}$, to calculate the corresponding average carrier lifetimes, $\tau_{avg} = \sum_i A_i\tau_i^2/A_i\tau_i$.[44,45] In this way, **Table 1** summarizes the parameters extracted from each TRPL curve. Accordingly, we obtained the shortest τ_{avg} for $CsPbBr_3@SiO_x$ PQDs, with a high contribution of radiative recombination (τ_1) and diminished non-radiative channel contribution (τ_2). This corresponds with the high PLQY of the photomaterial, corroborating the efficient ligand passivation of defects produced by ligands (APTES and OA) in the PQDs surface. In addition, by mediating the anion exchange process with CsX incorporation, some changes are appreciated in the PL dynamics of PQDs. In this context, the addition of Cl^- and I^- to obtain $CsPbCl_{3-x}Br_x@SiO_x$ and $CsPbBr_{3-x}I_x@SiO_x$ PQDs, respectively, induce a longer τ_{avg} and a decrease in the radiative recombination contribution. We deduce that the presence of deep energy states from chloride and the low complexation affinity of Pb—I bonds compared to intrinsic Pb—Br ones favor the appearance of a more defective perovskite structure,[4] which is in line with the lower PLQY values for these samples. Then, to analyze the carrier recombination dynamics of $CsPbX_3@SiO_x$ PQDs colloidal solutions, we determined the radiative and non-radiative recombination constants (k_r, k_{nr}, and their k_{nr}/k_r ratio), see Figure 2B,C, by using the PLQY and τ_{avg} values obtained from TRPL measurements, see Table 1. The results point out that $CsPbBr_3@SiO_x$ PQDs show a predominance of emission via radiative channels over non-radiative pathways (high k_r, low k_{nr}, and k_{nr}/k_r ratio), concluding that the LARP synthesis of this kind of PQDs in presence of APTES is suitable for achieving an efficient amino-functionalized SiO_x coverage, suppressing structural defects sites. On the contrary, the favored non-radiative pathway over radiative mechanism (low k_r, high k_{nr}, and k_{nr}/k_r ratio) for $CsPbCl_{3-x}Br_x@SiO_x$ and $CsPbBr_{3-x}I_x@SiO_x$ PQDs is attributed to the formation of deep energy states and the emergence of halide defects induced by direct Cl^- and I^-exchange beyond the SiO_x shell, respectively. As halide ions diffuse through the SiO_x shell, we speculate that the coordination between APTES (through ammonium cation) and the halides become weakened, leading to the formation of carrier traps for quenching the PL features.

To rationalize the surface chemistry of $CsPbX_3@SiO_x$ PQDs colloidal solutions, X-ray photoelectron spectroscopy (XPS) measurements were performed. As seen in the survey spectra of

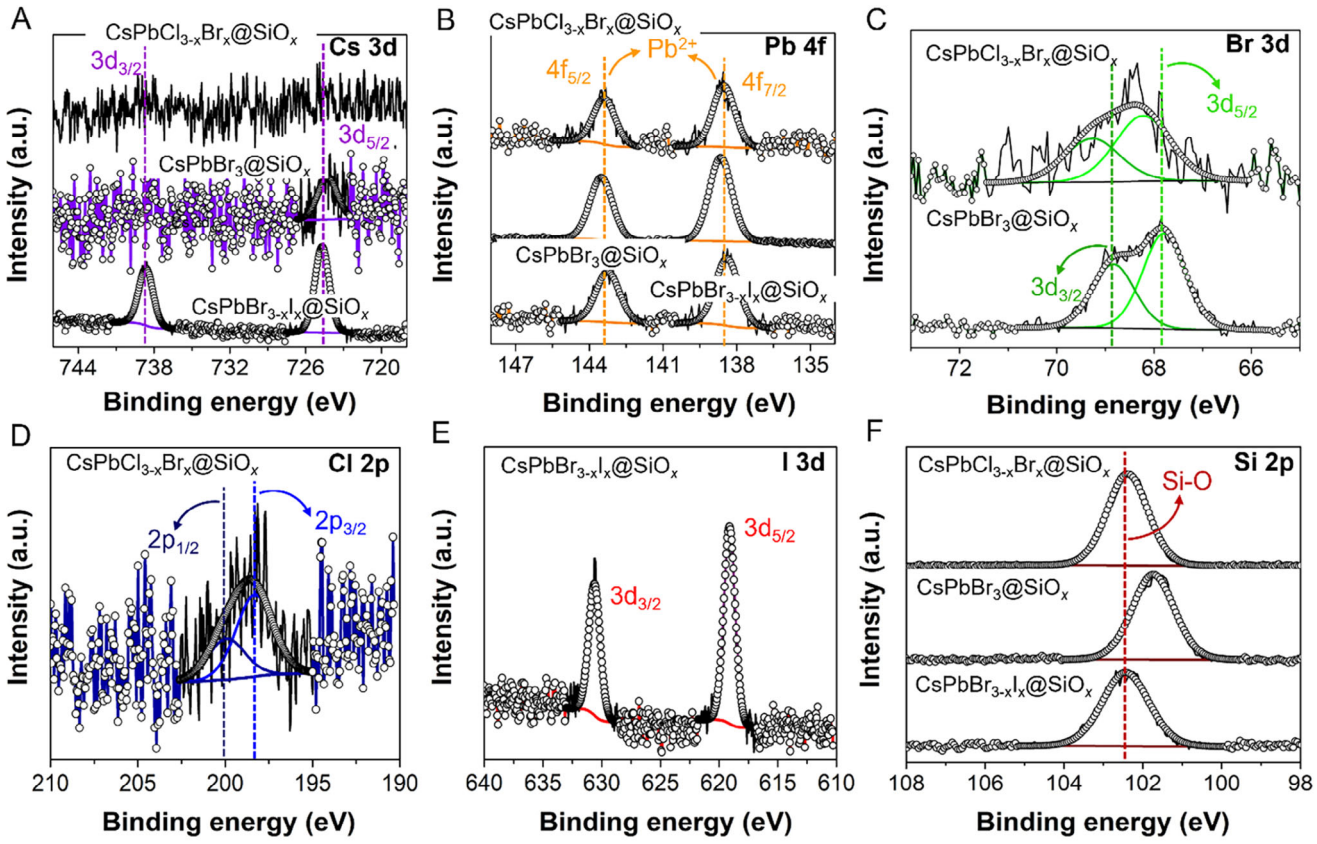

Figure 3. HR-XPS (A) Cs 3d, (B) Pb 4f, (C) Br 3d, (D) Cl 2p, (E) I 3d, and (F) Si 2p of $CsPbX_3@SiO_x$ PQDs.

respective samples, elements such as C, N, O, Cs, Pb, Si, Cl, Br, and I were identified, see Figure S8 (Supporting Information). A summary of the chemical composition of PQDs is exhibited in Table S2 (Supporting Information). **Figure 3A** shows the high-resolution (HR)-XPS Cs 3d spectra of $CsPbX_3@SiO_x$ PQDs, where a doublet at ≈724/738 eV was obtained. These signals are ascribed to Cs $3d_{5/2}$ and $3d_{3/2}$ core levels.[47] Simultaneously, the HR-XPS Pb 4f spectra of materials were achieved, see Figure 3B, exhibiting the typical doublet at ≈138/143 eV, attributed to Pb $4f_{7/2}$ and $4f_{5/2}$ core levels, from the Pb^{2+} contained into the $[PbX_6]^{4-}$ octahedra units.[4] Concerning the halide composition, $CsPbBr_3@SiO_x$ and $CsPbCl_{3-x}Br_x@SiO_x$ PQDs display the HR-XPS Br 3d spectra, see Figure 3C, where the Br $3d_{5/2}$ and $3d_{3/2}$ core levels located at ≈68/69 eV, corresponding to the Br^- contained into the Pb-Br bonds from the inorganic layers.[48] In addition, the HR-XPS Cl 2p spectrum appears in the mixed Cl/Br-perovskite, evidencing the typical Cl $2p_{3/2}$ and $2p_{1/2}$ core levels at ≈198/200 eV, see Figure 3D, attributed to the co-existence of Cl^- forming Pb-Cl bonds.[4] At this point, Br 3d signals from the mixed Cl/Br-perovskite are shifted to higher binding energies (BEs) considering the higher electronegativity of chloride than bromide into the octahedra units. Lastly, the HR-XPS I 3d is obtained from the $CsPbBr_{3-x}I_x@SiO_x$ PQDs, visualizing the I $3d_{5/2}$ and $3d_{3/2}$ core levels at ≈619/631 eV, respectively, see Figure 3E, ascribed to the presence of I^- composing the Pb-I bonds.[49,50] In all the samples, the HR-XPS Si 2p spectra are obtained, showing a single peak at 102 eV, see Figure 3F. This signal is associated with the Si-O bonds from the SiO_x shell.[49] Interestingly, the Si 2p spectrum of pure $CsPbBr_3@SiO_x$ was displaced to lower BEs, possibly by the incorporation of a lower oxygen content into the perovskite, indicating a better structural integrity in the perovskite. On the other hand, the Br 3d signal was not evidenced in

Table 1. Determination of radiative and non-radiative recombination decay rate constants, k_r and k_{nr}, respectively by fitting the time-resolved PL decays of $CsPbX_3@SiO_x$ PQDs to a bi-exponential function $PL = y_0 + A_1e^{-x/\tau_1} + A_2e^{-x/\tau_2}$,[46] shown in Figure 2A. Expressions used in the calculations: $\tau_{avg} = (\Sigma A_i\tau_i^2/\Sigma A_i\tau_i)$, $\tau_{avg} = 1/(k_r+k_{nr})$ and $k_r = (PLQY/\tau_{avg})$.[4] PLQY values were used in the 0–1 range.

Perovskite	A1	τ1 [ns]	A2	τ2 [ns]	τavg [ns]	PLQY	*kr* [x 10^7 s^{-1}]	*knr* [x 10^7 s^{-1}]	*knr/kr ratio*
CsPbCl3-xBrx@SiO*x*	0.86	4.5	0.14	20	11	0.115	1.04	8.05	7.74
CsPbBr3@SiO*x*	0.94	5.6	0.06	18.2	7.9	0.993	12.6	0.0875	0.00694
CsPbBr3-xIx@SiO*x*	0.81	13	0.19	33.4	20.7	0.302	1.46	3.37	2.31

$CsPbBr_{3-x}I_x@SiO_x$ PQDs, since an excess of iodide species was estimated through the chemical composition, see Table S2 (Supporting Information).

Since iodide is more labile than bromide anions, the former can diffuse faster to the PQDs, favoring their accumulation at the interface, between perovskite core and SiO_x shell. This fact, together with the existence of a thick SiO_x shell (8 and 9 nm coverage) allows us to deduce that bromide species cannot be easily detected since the XPS analysis penetration depth is around 10 nm and the majority of signal is obtained in around 1–2 nm, from the surface. This affirmation can also be supported by a low estimated fraction of all the elements from the PQDs, mainly Cs, which is low and absent in $CsPbBr_3@SiO_x$ and $CsPbCl_{3-x}Br_x@SiO_x$ PQDs, respectively, see Figure 3A. Then, the emergence of Cs^+ defects and the presence of a high Cl fraction in the material surface after the halide exchange allow to suggest that some chloride vacancies are formed in the Cl/Br-perovskite core, inducing the formation of deep states, which can explain the favored nonradiative carrier recombination in the Cl/Br-perovskite. On the contrary, $CsPbBr_{3-x}I_x@SiO_x$ PQDs exhibit an excess of Cs^+ content, in agreement with the high iodide content estimated for this material. However, the fact that a lower PLQY (ascribed to a restrained radiative recombination) is observed for this material compared with $CsPbBr_3@SiO_x$ PQDs allows to deduce that a fraction of iodide species can diffuse out from the perovskite structure after the anion exchange process, considering the low complexation affinity of Pb-I bond, unbalancing the surface stoichiometry of the mixed Br/I-perovskite. Lastly, the fact that Cl^- and I^- species migrate to reach $CsPbBr_3$ PQDs core indicates that SiO_x shell is permeable enough to promote anion-exchange and produce the respective mixed halide PQDs, suggesting that silica pores are larger than the size of halide species.[51,52] In conclusion, the halide exchange process can generate a high density of defect sites in the $CsPbX_3@SiO_x$, being caused by the ion permeation of the SiO_x shell, hampering the photophysical properties of the final product.

With the purpose of understanding the formation of a SiO_x shell covering the PQDs, a chemical mechanism can be established. After incorporating the main reagents such as CsBr, $PbBr_2$ as the building blocks for perovskite growth, APTES and EG are also introduced into the mixture reaction in DMF, being the pivotal ligands for material stabilization. Here, hydrolysis and condensation of APTES and EG are promoted, inducing the emergence of -Si-O-Si- and -Si-O-C_2H_4-O-Si- linkages, also mediating the complexation reactions to produce Si-O-Pb and C_2H_4-O-Pb coordination bonds. In this context, while the APTES content controls the density of connected -Si-O-Si- networks, which modulates the SiO_x shell thickness, the EG content tailors the density of elongated -Si-O-C_2H_4-O-Si- linkages, regulating directly the perovskite core size. Therefore, we propose LARP method as promising alternative to obtain single SiO_x-covered PQDs with modulable core–shell sizes.

After characterization of synthesized $CsPbX_3@SiO_x$ PQDs, we have evaluated their application potentiality. A significant challenge with PQDs has been their lack of water resistance. To test their stability against water, $CsPbBr_3@SiO_x$ PQDs in the form of films were prepared with and without a post-annealing process at 100 °C for 30 min, taking advantage of the low permeability of the SiO_x coverage. The annealing process does not produce any change in the crystalline phase, as we highlighted through X-ray diffraction (XRD) patterns of PQDs films with and without thermal treatment, see Figure S9 (Supporting Information). Both films showed a cubic perovskite structure (ICSD 00-054-075).[53] The broad hump observed ≈ 15° to 20° suggests the presence of amorphous silica within $CsPbBr_3@SiO_x$ PQDs, similar to our earlier study.[40] In addition, the post-synthetic annealing does not alter the SiO_x shell integrity neither since we estimated its thickness by calculating the sizes of both PQDs core and entire $CsPbBr_3@SiO_x$ nanoparticles through typical TEM images, see Figure S10A–D (Supporting Information). Here, the PQDs core and entire nanoparticle exhibit sizes of 9.2 ± 1.2 nm and 27.1 ± 1.9 nm, respectively, with an average SiO_x shell thickness ≈9.0 ± 2.2 nm. The similarity between the core–shell sizes before and after annealing process indicates that SiO_x coverage is no longer modified after annealing, enhancing their uniformity (less error in SiO_x thickness) possibly attributed to the sealing of some silica pores.

Then, films were respectively immersed in deionized (DI) water and measured by UV–vis absorption and PLQY measurements, see **Figure** 4A,B. The relative PLQY was estimated based on the integrated values of each PL emission spectra measured while these films were immersed in DI water. At this point, both the relative absorption and PLQY features of annealed film were reduced slower compared with the non-annealed sample after 5 h of immersion. Interestingly, although the SiO_x shell pores are sufficiently large to allow the diffusion of Cl^- and I^- anions to reach the $CsPbBr_3$ PQDs, producing the corresponding $CsPbCl_{3-x}Br_x@SiO_x$ and $CsPbBr_{3-x}I_x@SiO_x$ PQDs, this silica coverage is enough to delay the eventual perovskite deterioration by effect of H_2O molecules. Then, after annealing the PQDs film, it is possible to partially seal the shell pores, restraining even more the mobility of H_2O toward the PQDs. This partially sealed SiO_x coverage is not fully impermeable. We observed an increase in the PLQY values of the annealed sample during the first 20 min, see Figure 4B, indicating that the low density of diffused H_2O can interact with the perovskite surface, mediating the surface passivation through the oxygen incorporation and removing defect sites.[54,55] Accordingly, our single $CsPbBr_3@SiO_x$ PQDs shows a competitive water stability, retaining ≈45% of initial PL, compared with the state-of-the-art, for instance, analogous $CsPbBr_3@SiO_x$ PQDs encapsulated with polyvinylpyrrolidone (PVP) and n-isopropylacrylamide with a lower H_2O resistance up to 1 h, retaining between 20–75% of initial PL,[56] $MAPbBr_3$ PQDs encapsulated with cucurbit[7]- uril-adamantyl ammonium complex with water stability up to 2 h, exhibiting a considerable emission decrease, retaining ≈13% of initial PL,[57] and comparable with cross-linked oleylammonium encapsulated $CsPbBr_3$ PQDs by using Ar-O_2 plasma treatment, depicting a retaining ≈50% of initial PL after 6 h of water soaking.[58] Therefore, we deduce that the material offers enhanced thermal and water long-term stability, which can be beneficial to conduct potential solar-driven chemical reactions in future contributions.

The increased water resistance of the prepared $CsPbBr_3@SiO_x$ PQDs films makes this material interesting for scale up film preparation processes like inkjet printing.[59–61] For a successful inkjet printing process, the size of the dispersed nanomaterials in the ink should be smaller than 1/50 of the nozzle diameter (δ) to prevent nozzle clogging. The quality and homogeneity of the

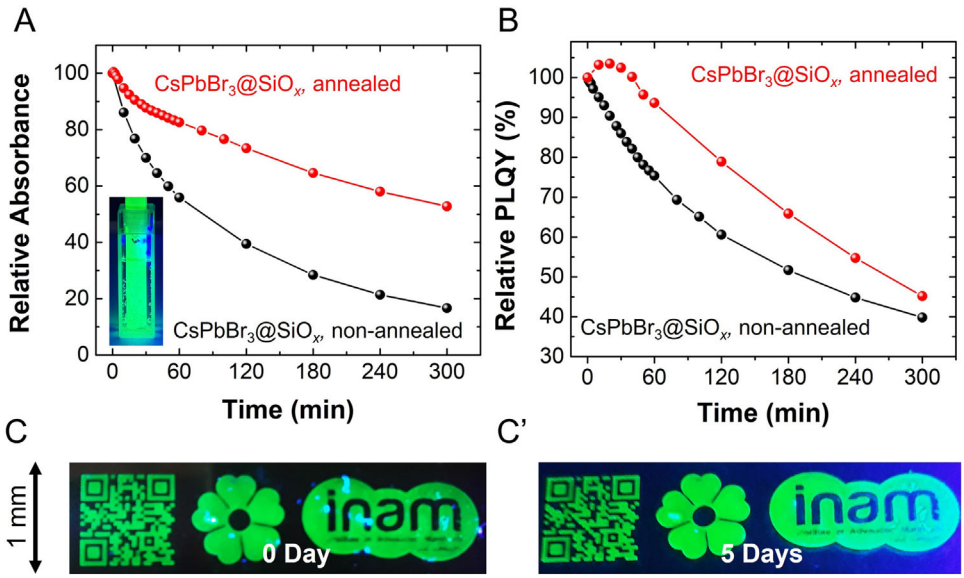

Figure 4. A) Relative absorbance by measuring UV–vis. absorption spectroscopy and B) Relative PLQY of $CsPbBr_3@SiO_x$ PQDs films with and without the post-annealing process in water for 5 h. C,C') luminescent patterns prepared by an inkjet-printed $CsPbBr_3@SiO_x$ PQDs ink on a transparent glass substrate under UV light at (C) 0 and (C') 5 days exposed to ambient air.

ejected droplet are influenced by rheological parameters such as density (ρ), viscosity (η), and surface tension (γ), which respectively correspond to inertial, viscous, and surface tension forces. These parameters are crucial for determining the dimensionless figure of merit (FOM) Z number, which is expressed by Equation (1) and is equivalent to the inverse of the Ohnesorge (Oh) number, independent of fluid velocity (1):

$$Z = \frac{1}{Oh} = \frac{\sqrt{\delta\rho\gamma}}{\eta} \quad (1)$$

The Z value should be comprised between 1 and 14 for obtaining stable droplets during printing, although the optimal Z value depends on the printing cartridges, in our case, piezoelectric Samba printing cartridges using a Suss LP50 Pixdro inkjet printer.[62,63] After synthesis, the $CsPbBr_3@SiO_x$ PQDs are redispersed in chlorobenzene with a concentration of 10 mg·mL^{-1}. This solution is unsuitable for inkjet printing due to low viscosity ($Z > 22$) and printing resolution is expected to be low due to the high evaporation rate of the solvent (1.1 versus butyl acetate). Thus, for improving the printing process and avoiding the coffee ring formation during the drop drying after printing, a secondary higher viscosity and higher-boiling-point co-solvent was studied, which also must be chemically compatible with the PQDs. The best rheological results were obtained preparing a mixture of the PQDs in chlorobenzene and terpineol in a 1:1 volume ratio ($Z = 13.6$), resulting in a final PQDs concentration of 5 mg mL^{-1}, see Table S1 (Supporting Information). Accordingly, the formation of a stable droplet is expected, allowing the formation of stable luminescent printed patterns with complex forms, including a QR code of the Technological Transfer Unity website of the Institute of Advanced Materials (INAM), see Figure 4C. On the other hand, the SiO_x-covered PQDs synthesized in our work can produce a suitable ink for inkjet printing process at lower concentrations (5 mg mL^{-1}) with a comparable viscosity than reported $CsPbBr_3$ PQDs synthesized by conventional hot-injection method and deposited on poly-(9-vinylcarbazole) layer, where a concentration as high as 15 mg mL^{-1} is required to obtain a viscosity in between 0.62-1.46 in presence of toluene/dodecane solvents[64] and bulky alkylammonium bromide coated FA-doped $CsPbBr_3$ PQDs at same concentration (15 mg mL^{-1}) generating a vicosity between 0.79-1.70 into using different n-octane:n-dodecane mixtures.[65] In conclusion, $CsPbX_3@SiO_x$ PQDs show a facile way to modulate their optical features, opening the possibilities of preparing multicolor luminescent films and inks for future fabrication of optoelectronic devices and inkjet printing processes.

After analyzing the photophysical properties and stability features of $CsPbX_3@SiO_x$ PQDs, we investigated these materials for color-converting applications. For this purpose, we have embedded the corresponding as-prepared PQDs inks into a commercial epoxy resin and deposited the blend on a commercial LED chip (3 W and wavelength: 440–450 nm, see Figure S11A, Supporting Information for further details). Under the operation of the LED chips, part of the emission of the device is transmitted, while the rest of the light is absorbed by the PQDs active layers, converting it into blue-, green-, and red-emission. Then, we proceed to study the stability of luminescent LED chips along the time, analyzing the retention of the initial luminescence. For both blue and green color converters, blacklight from the commercial LED was filtered achieve the characteristic PL of active layers. As seen in **Figure** 5A,B, $CsPbCl_{3-x}Br_x@SiO_x$ and $CsPbBr_3@SiO_x$-LEDs generate a PL emission located at 487 and 520 nm, respectively. Then, $CsPbBr_3@SiO_x$-LED show a more stable PL emission (9 h) during the light conversion compared with $CsPbCl_{3-x}Br_x@SiO_x$ one (stable for 1.5 h), indication of a better surface protection in the Br-perovskite. Moreover, although a progressive decrease in the PL intensity in both of the systems is evidenced, being associated with some surface ligand detachment at prolonged

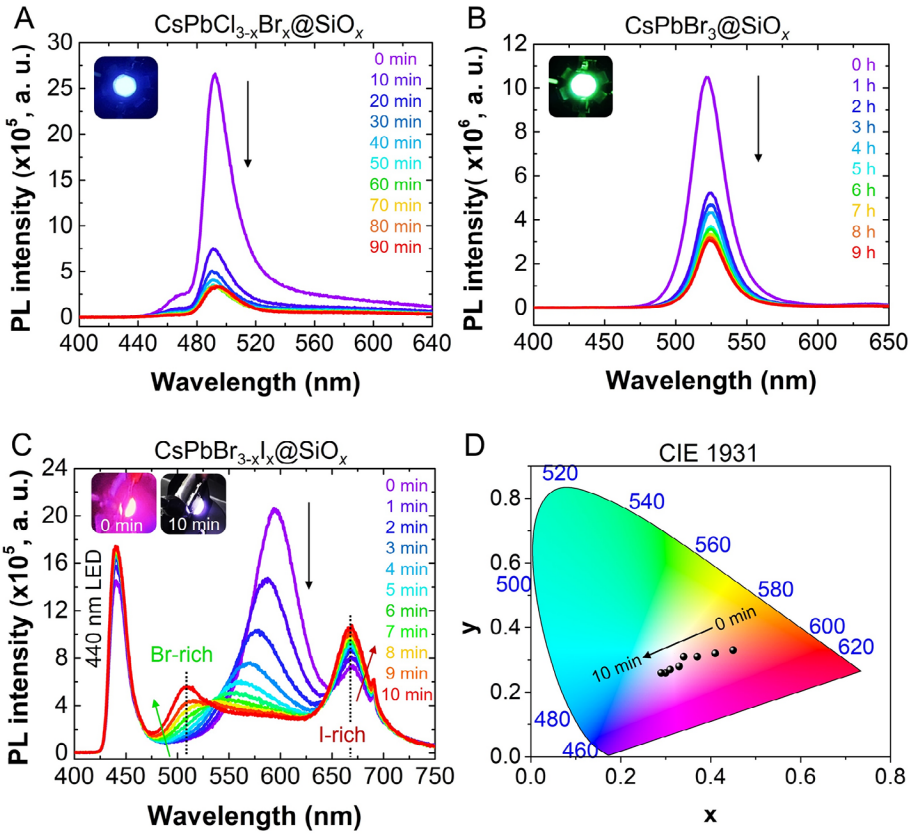

Figure 5. PL spectra of epoxy-resin covered A) blue-emitting $CsPbCl_{3-x}Br_x@SiO_x$, B) green-emitting $CsPbBr_3@SiO_x$, and C) red-emitting $CsPbBr_{3-x}I_x@SiO_x$, based LED devices by applying a constant voltage of 2.5 V along the operational time. D) Chromaticity diagram of $CsPbBr_{3-x}I_x@SiO_x$, LED under operation, showing the variation of white light tonality along time. Insets show the corresponding luminescent devices during the color conversion process.

irradiation flux (0.45 W cm^{-2}) at 2.5 V,[20] the PL intensity of the mixed Cl/Br-perovskite exhibits a faster decline than Br-perovskite. We attributed this behavior to the existence of Cl^- deep states in the former material.[4] This fact agrees with the optical features of the $CsPbCl_{3-x}Br_x@SiO_x$, where the deep energy states can promote material degradation.

On the other hand, during the continuous operation of $CsPbBr_{3-x}I_x@SiO_x$-LED, the initial emergence of two PL emissions at 593 and 667 nm is evidenced, see Figure 5C, attributed to the formation of two different I-rich domains into the perovskite active layer. Attending to the slow anion-exchange process to prepare this material, see in Figure 1C. SiO_x shell does not allow the permeation of a high density of iodide species to reach the $CsPbBr_3$, promoting the generation of a highly defective Br/I-perovskite structure. At this point, we propose that, after the Br/I-perovskite deposition onto the LED chip, nanoparticles are closer together, favoring the iodide diffusion under device operation and thereby generating the Br-rich and I-rich domains into the active layer (taking advantage of the good lability of iodide anions).[66,67] Then, after 10 min of continuous operation, the intensity of the long-wavelength PL in progressively increased, while a blueshift is noted in the shorter-wavelength PL emission to reach total quenching, with the simultaneous appearance of a new PL signal at 508 nm. This behavior indicates the generation of Br- and I-domains from the PL splitting of mixed halide, which is commonly associated to photoinduced phase segregation. However, after conducting this experiment under intermittent operation of the $CsPbBr_{3-x}I_x@SiO_x$-LED (this is by obtaining PL emission at 0 min, the LED was turned off during 20 min and then turned on for a couple of seconds for obtaining the PL emission, to observe halide segregation reversibility), see Figure S11B (Supporting Information), the PL behavior of the device was similar than that of the LED under continuous operation. This fact makes us discard any reversible halide separation. On the contrary, we can address that the SiO_x shell permeability can be exploited for triggering the interparticle iodide diffusion to cover the visible region of the energy spectrum by the appearance of PL splitting coming from the wide-bandgap Br-rich and low-bandgap I-rich domains.

The dual PL feature from the $CsPbBr_{3-x}I_x@SiO_x$ PQDs mediates the generation of white-light emission (using the blacklight of the commercial LED), achieving all the color tonalities along the time (cool, neutral and warm) as indicated through its chromaticity diagram, see Figure 5D, which can be preserved up to 2 h under intermittent LED operation before its final deterioration. At this point, if an optimized fabrication of the $CsPbBr_{3-x}I_x@SiO_x$-LED can be reached, it will be an attractive option to obtain RGB combination with commercial blacklight devices to modulate the generation of high-quality

white emission, ideal for LCD technologies. Therefore, we can conclude that the optical features of $CsPbX_3@SiO_x$ colloidal solutions can be controlled through composition engineering, improving their water/thermal resistance, with prominent potentiality as inks for the fabrication of color-converting LEDs, even generating white light emission from a single perovskite system.

3. Conclusion

Monodisperse $CsPbX_3@SiO_x$ core–shell PQDs are synthesized using a ligand-assisted reprecipitation method, showing a PLQY of up to 99.4% and uniform particle distribution. This indicates that the addition of APTES ligand can promote the efficient passivation of surface defect sites, improving the PL emission via radiative channels and hindering the emergence of non-radiative carrier traps. Then, it is also possible to mediate the anion exchange process between the $CsPbBr_3@SiO_x$ PQDs and Cl- and I-precursors, tailoring the photophysical properties such as the bandgap and producing mixed halide $CsPbCl_{3-x}Br_x@SiO_x$ and $CsPbBr_{3-x}I_x@SiO_x$ PQDs. Nevertheless, the diffusion of chloride and iodide induces structural defects in the host $CsPbBr_3$ PQDs core, considering the low permeability of the SiO_x shell. Precisely, the formation of a thick SiO_x layer does not allow for the detection of the complete chemical composition of the PQDs, ensuring that most of the diffused halide is accumulated in the composite surface. In this context, we infer that SiO_x shell pores are large enough to favor the diffusion of chloride to reach the perovskite core compared to iodide species, which is the reason for taking a longer time for halide exchange. At this point, both the formation of deep energy states by the presence of Cl^- and the high lability of I^- species, generating halide vacancies, are the main explanations to evidence the non-radiative recombination as the main PL dynamics in the mixed Cl/Br- and Br/I-perovskite, producing a lower PLQY than pure $CsPbBr_3@SiO_x$ PQDs. On the other hand, by carrying out a thermal process to PQDs films, long-term stability in water is favored, hindering the diffusion of H_2O to reach the perovskite core. Simultaneously, the low density of available water molecules can passivate the surface defect sites in the perovskite, producing an initial increase of the PL and restraining the fast material deterioration. Then, by reaching a suitable combination between PQDs and low/high boiling point solvents, we can obtain $CsPbBr_3@SiO_x$ inks to perform inkjet printing applications, generating stable luminescent patterns with complex geometries. Lastly, these inks can also be used as active layers for the fabrication of color converting LEDs with operational stability of up to 9 h, where their PL emission can be controlled through the composition engineering, even achieving white emission from a single $CsPbX_3@SiO_x$ system. Therefore, the synthesis of $CsPbX_3@SiO_x$ PQDs by the LARP synthetic route provides a high potential to be applied in solar-driven chemistry and inkjet printing, which can facilitate the future fabrication of optoelectronic devices.

Supporting Information

Supporting Information is available from the Wiley Online Library or from the author.

Acknowledgements

This research was supported by the National Research Foundation of Korea grant funded by the Korean Government (2022R1C1C1011860, RS-2024-00441659). This work was also supported by the Ministry of Science and Innovation of Spain MCIN/AEI/10.13039/501100011033/ and by FEDER "Una manera de hacer Europa" under ProjectConFlex (PID2023-151880OB-C33). A.F.G.-R. thanks to ANID for the financial support through the FONDECYT Iniciación Project (Grant n°11240161), and through the Vinculación International Project (FOVI240255). S.J.Y. and J.P. also acknowledge to Korea Basic Science Institute (National Research Facilities and Equipment Center) grant funded by the Ministry of Education (2020R1A6C101B194) for utilizing characterization tools. The authors acknowledge the Ministry of Education, Youth and Sports of the Czech Republic, for the financial support of XPS measurements using the CEMNAT infrastructure (project LM 2023037). J.S.C. and A.F.G.R. thank the financial support provided by the Generalitat Valenciana via European Union-NextGeneration EU project (Print-P). F.P. thanks the financial support provided by the Generalitat Valenciana via Prometeo Grant Q-Solutions (CIPROM/2021/078). C.P.R. thanks the financial support provided by the European Union by the project HORIZON-CL5-2022-D3-03-05 GA 101122345. S.M. acknowledges the Universitat Jaume I project UJI-2023-01.

Conflict of Interest

The authors declare no conflict of interest.

Author Contributions

S.Y.P., G.S., and T.K. contributed equally to this work. A.F.G.-R., S.J.Y., and I.M.-S. proposed overall study. S.Y.P., H.J., A.F.G.-R., and S.J.Y. designed the experiments. S.Y.P. and Y.K. synthesized the PQDs, S.Y.P., G.S., T.K., J.S., B.K., J.P., J.H.B., and H.J. conducted the optical, morphological, structural, and surface chemistry characterization. J.S. carried out the study of inkjet printing conditions and preparation of corresponding PQDs inks. J.R.-P. contributed to the XPS measurements and analysis. C.P.-R., S.M., F.P., and I.U.-A. contributed to the analysis of material characterization. All authors contributed to writing the manuscript and the discussions.

Data Availability Statement

The data that support the findings of this study are available from the corresponding author upon reasonable request.

Keywords

anion-exchange, color converters, core–shell PQDs, ligand passivation, thermal/water stability

Received: March 27, 2025
Revised: July 27, 2025
Published online:

[1] Y.-K. Wang, F. Yuan, Y. Dong, J.-Y. Li, A. Johnston, B. Chen, M. I. Saidaminov, C. Zhou, X. Zheng, Y. Hou, K. Bertens, H. Ebe, D. Ma, Z. Deng, S. Yuan, R. Chen, L. K. Sagar, J. Liu, J. Fan, P. Li, X. Li, Y. Gao, M.-K. Fung, Z.-H. Lu, O. M. Bakr, L.-S. Liao, E. H. Sargent, *Angew. Chem., Int. Ed.* **2021**, *60*, 16164.
[2] Y. Zeng, W. Chen, Y. Deng, W. Gu, C. Wu, Y. Guo, P. Huang, F. Liu, H. Li, *ACS Appl. Nano Mater.* **2022**, *5*, 9534.

[3] P. Serafini, A. Villanueva-Antolí, S. D. Adhikari, S. Masi, R. S. Sánchez, J. Rodriguez-Pereira, B. Pradhan, J. Hofkens, A. F. Gualdrón-Reyes, I. Mora-Seró, *Chem. Mater.* **2023**, *35*, 3998.
[4] C. Lee, Y. Shin, A. Villanueva-Antolí, S. Das Adhikari, J. Rodriguez-Pereira, J. M. Macak, C. A. Mesa, S. Giménez, S. J. Yoon, A. F. Gualdrón-Reyes, I. Mora-Seró, *Chem. Mater.* **2021**, *33*, 8745.
[5] J. Xue, J.-W. Lee, Z. Dai, R. Wang, S. Nuryyeva, M. E. Liao, S.-Y. Chang, L. Meng, D. Meng, P. Sun, O. Lin, M. S. Goorsky, Y. Yang, *Joule* **2018**, *2*, 1866.
[6] A. Swarnkar, A. R. Marshall, E. M. Sanehira, B. D. Chernomordik, D. T. Moore, J. A. Christians, T. Chakrabarti, J. M. Luther, *Science* **2016**, *354*, 92.
[7] Z. Zolfaghari, E. Hassanabadi, D. Pitarch-Tena, S. J. Yoon, Z. Shariatinia, J. van de Lagemaat, J. M. Luther, I. Mora-Seró, *ACS Energy Lett.* **2018**, *4*, 251.
[8] C. Zhou, J. Yu, H. Dong, F. Yuan, X. Zheng, M. Jiang, L. Zhang, *J. Mater. Chem. C* **2020**, *8*, 13642.
[9] G. Getachew, A. Wibrianto, A. S. Rasal, W. Batu Direrssa, J.-Y. Chang, *Coord. Chem. Rev.* **2023**, *482*, 215073.
[10] H. Lian, Y. Li, S. Saravanakumar, H. Jiang, Z. Li, J. Wang, L. Xu, W. Zhao, G. Han, *Coord. Chem. Rev.* **2022**, *452*, 214313.
[11] J. De Roo, M. Ibáñez, P. Geiregat, G. Nedelcu, W. Walravens, J. Maes, J. C. Martins, I. Van Driessche, M. V. Kovalenko, Z. Hens, *ACS Nano* **2016**, *10*, 2071.
[12] A. F. Gualdrón-Reyes, D. F. Macias-Pinilla, S. Masi, C. Echeverría-Arrondo, S. Agouram, V. Muñoz-Sanjosé, J. Rodríguez-Pereira, J. M. Macak, I. Mora-Seró, *J. Mater. Chem. C* **2021**, *9*, 1555.
[13] S. Ji, X. Yuan, S. Cao, W. Ji, H. Zhang, Y. Wang, H. Li, J. Zhao, B. Zou, *J. Phys. Chem. Lett.* **2020**, *11*, 2142.
[14] I. Levchuk, A. Osvet, X. Tang, M. Brandl, J. D. Perea, F. Hoegl, G. J. Matt, R. Hock, M. Batentschuk, C. J. Brabec, *Nano Lett.* **2017**, *17*, 2765.
[15] L. Dai, Z. Deng, F. Auras, H. Goodwin, Z. Zhang, J. C. Walmsley, P. D. Bristowe, F. Deschler, N. C. Greenham, *Nat. Photonics* **2021**, *15*, 696.
[16] S. Min, M. Jeon, J. Cho, J. H. Bang, P. V. Kamat, *Nano Converg.* **2024**, *11*, 49.
[17] A. Dey, J. Ye, A. De, E. Debroye, S. K. Ha, E. Bladt, A. S. Kshirsagar, Z. Wang, J. Yin, Y. Wang, L. N. Quan, F. Yan, M. Gao, X. Li, J. Shamsi, T. Debnath, M. Cao, M. A. Scheel, S. Kumar, J. A. Steele, M. Gerhard, L. Chouhan, K. Xu, X.-G. Wu, Y. Li, Y. Zhang, A. Dutta, C. Han, I. Vincon, A. L. Rogach, et al., *ACS Nano* **2021**, *15*, 10775.
[18] K. H. Fausia, B. Nharangatt, R. N. Vinayakan, A. R. Ramesh, V. Santhi, K. R. Dhandapani, T. P. Manoj, R. Chatanathodi, D. Jose, K. Sandeep, *ACS Omega* **2024**, *9*, 8417.
[19] S. Masi, A. F. Gualdrón-Reyes, I. Mora-Seró, *ACS Energy Lett.* **2020**, *5*, 1974.
[20] R. An, F. Zhang, X. Zou, Y. Tang, M. Liang, I. Oshchapovskyy, Y. Liu, A. Honarfar, Y. Zhong, C. Li, H. Geng, J. Chen, S. E. Canton, T. Pullerits, K. Zheng, *ACS Appl. Mater. Interfaces* **2018**, *10*, 39222.
[21] D. Yang, X. Li, W. Zhou, S. Zhang, C. Meng, Y. Wu, Y. Wang, H. Zeng, *Adv. Mater.* **2019**, *31*, 1900767.
[22] F. Krieg, P. C. Sercel, M. Burian, H. Andrusiv, M. I. Bodnarchuk, T. Stöferle, R. F. Mahrt, D. Naumenko, H. Amenitsch, G. Rainò, M. V. Kovalenko, *ACS Cent. Sci.* **2020**, *7*, 135.
[23] C.-H. Kuan, S.-H. Yang, *Mater. Adv.* **2022**, *3*, 7824.
[24] S. Das Adhikari, A. F. Gualdrón Reyes, S. Paul, J. Torres, B. Escuder, I. Mora-Seró, S. Masi, *Chem. Sci.* **2023**, *14*, 8984.
[25] X. Li, M. Ibrahim Dar, C. Yi, J. Luo, M. Tschumi, S. M. Zakeeruddin, M. K. Nazeeruddin, H. Han, M. Grätzel, *Nat. Chem.* **2015**, *7*, 703.
[26] Y. Lu, F. Alam, J. Shamsi, M. Abdi-Jalebi, *J. Phys. Chem. C* **2024**, *128*, 10084.
[27] Y. Zheng, Y. Duan, Y. Ye, X. Zheng, A. Du, E. Chen, S. Xu, T. Guo, *Luminescence* **2024**, *39*, 4691.
[28] K. He, D. Chen, L. Yuan, J. Xu, K. Xu, J. Hu, S. Liang, H. Zhu, *Chem. Eng. J.* **2024**, *480*, 148066.
[29] L. Yang, B. Fu, X. Li, H. Chen, L. Li, *J. Mater. Chem. C* **2021**, *9*, 1983.
[30] W. Yang, F. Gao, Y. Qiu, W. Liu, H. Xu, L. Yang, Y. Liu, *Adv. Opt. Mater.* **2019**, *7*, 1900546.
[31] Z. Liu, L. Sinatra, M. Lutfullin, Y. P. Ivanov, G. Divitini, L. De Trizio, L. Manna, *Adv. Energy Mater.* **2022**, *12*, 2201948.
[32] Y. He, L. Zhang, G. Chen, Y. Liu, S. Shi, P. Jiang, J. Ding, S. Xu, C. Geng, *Appl. Surf. Sci.* **2023**, *611*, 155724.
[33] E. Mei, X. Liu, Y. Chen, Y. Yu, Z. Chen, K. Yang, X. Liang, W. Xiang, *Appl. Surf. Sci.* **2021**, *569*, 150964.
[34] P. Nuket, Y. Akaishi, G. Yoshimura, T. Kida, P. Vas-Umnuay, *Ceram. Int.* **2022**, *48*, 32504.
[35] C. Jia, H. Li, X. Meng, H. Li, *Chem. Commun.* **2018**, *54*, 6300.
[36] B. Qiao, P. Song, J. Cao, S. Zhao, Z. Shen, G. Di, Z. Liang, Z. Xu, D. Song, X. Xu, *Nanotechnology* **2017**, *28*, 445602.
[37] B. Wang, C. Zhang, S. Huang, Z. Li, L. Kong, L. Jin, J. Wang, K. Wu, L. Li, *ACS Appl. Mater. Interfaces* **2018**, *10*, 23303.
[38] Q. Zhong, M. Cao, H. Hu, D. Yang, M. Chen, P. Li, L. Wu, Q. Zhang, *ACS Nano* **2018**, *12*, 8579.
[39] X. Tang, W. Chen, Z. Liu, J. Du, Z. Yao, Y. Huang, C. Chen, Z. Yang, T. Shi, W. Hu, Z. Zang, Y. Chen, Y. L. Ultrathin, *Small* **2019**, *15*, 1900484.
[40] S. J. Lee, Y. J. Lee, S. Seo, H. Jeon, D. Han, H. Im, N. K. Shrestha, S. J. Yoon, *J. Phys. Chem. C* **2022**, *126*, 7910.
[41] S. Fiorito, M. Silvestri, M. Cirignano, A. Marini, F. Di Stasio, *ACS Appl. Nano Mater.* **2024**, *7*, 3724.
[42] C.-W. Hsieh, R. K. Singh, S. Som, C.-H. Lu, *Chem. Eng. J. Adv.* **2022**, *12*, 100358.
[43] M. I. Bodnarchuk, S. C. Boehme, S. ten Brinck, C. Bernasconi, Y. Shynkarenko, F. Krieg, R. Widmer, B. Aeschlimann, D. Günther, M. V. Kovalenko, I. Infante, *ACS Energy Lett.* **2018**, *4*, 63.
[44] K. Cho, Y. Park, H. Jo, S. Seo, J. Moon, S. J. Lee, S. Y. Park, S. J. Yoon, J. Park, *J. Phys. Chem. Lett.* **2024**, *15*, 5795.
[45] T.-Y. Kim, B. S. Kim, J. G. Oh, S. C. Park, J. Jang, T. W. Hamann, Y. S. Kang, J. H. Bang, S. Giménez, Y. S. Kang, *ACS Appl. Mater. Interfaces* **2021**, *13*, 6208.
[46] X. Shen, Y. Zhang, S. V. Kershaw, T. Li, C. Wang, X. Zhang, W. Wang, D. Li, Y. Wang, M. Lu, L. Zhang, C. Sun, D. Zhao, G. Qin, X. Bai, W. W. Yu, A. L. Rogach, *Nano Lett.* **2019**, *19*, 1552.
[47] A. F. Gualdrón-Reyes, J. Rodríguez-Pereira, E. Amado-González, J. Rueda-P, R. Ospina, S. Masi, S. J. Yoon, J. Tirado, F. Jaramillo, S. Agouram, V. Muñoz-Sanjosé, S. Giménez, I. Mora-Seró, *ACS Appl. Mater. Interfaces* **2020**, *12*, 914.
[48] J. Zhu, Y. Zhu, J. Huang, Y. Gong, J. Shen, C. Li, *J. Mater. Chem. C* **2019**, *7*, 7201.
[49] K. He, C. Shen, Y. Zhu, X. Chen, Z. Bi, T. Marimuthu, G. Xu, X. Xu, *Langmuir* **2020**, *36*, 10210.
[50] J. Rodriguez-Pereira, J. Tirado, A. F. Gualdrón-Reyes, F. Jaramillo, R. Ospina, *Surface Sci. Spectra* **2020**, *27*, 024003.
[51] C. Rossi, R. Scarfiello, R. Brescia, L. Goldoni, G. Caputo, L. Carbone, D. Colombara, L. De Trizio, L. Manna, D. Baranov, *Chem. Mater.* **2021**, *34*, 405.
[52] M. Li, X. Zhang, P. Yang, *Nanoscale* **2021**, *13*, 3860.
[53] H. Shi, Q. Zhang, P. Shi, X. Zhang, *Appl. Phys. Lett.* **2020**, *117*, 261903.
[54] J. Jang, Y. H. Kim, S. Park, D. Yoo, H. Cho, J. Jang, H. B. Jeong, H. Lee, J. M. Yuk, C. B. Park, D. Y. Jeon, Y. H. Kim, B. S. Bae, T. W. Lee, *Adv. Mater.* **2020**, *33*, 2005255.
[55] H. Zhou, J. Park, Y. Lee, J. M. Park, J. H. Kim, J. S. Kim, H. D. Lee, S. H. Jo, X. Cai, L. Li, X. Sheng, H. J. Yun, J. W. Park, J. Y. Sun, T. W. Lee, *Adv. Mater.* **2020**, *32*, 2001989.
[56] M. R. Kar, U. Patel, S. Bhaumik, *Mater. Adv.* **2022**, *3*, 8629.
[57] S. Gonzalez-Carrero, L. Francés-Soriano, M. González-Béjar, S. Agouram, R. E. Galian, J. Pérez-Prieto, *Small* **2016**, *12*, 5245.

[58] R. Rathod, R. Das, M. R. Das, P. K. Santra, *ACS Appl. Nano Mater.* **2022**, *5*, 9852.
[59] B. Derby, *Annu. Rev. Mater. Res.* **2010**, *40*, 395.
[60] Z. Zhang, Z. Li, Y. Chen, Z. Zhang, K. Fan, S. Chen, L. Liu, S. Chen, *ACS Photonics* **2023**, *10*, 3435.
[61] G. Vescio, J. L. Frieiro, A. F. Gualdrón-Reyes, S. Hernández, I. Mora-Seró, B. Garrido, A. Cirera, *Adv. Mater. Technol.* **2022**, *7*, 2101525.
[62] T. D. Grant, A. C. Hourd, S. Zolotovskaya, J. B. Lowe, R. J. Rothwell, T. D. A. Jones, A. Abdolvand, *Mater. Des.* **2022**, *214*, 110377.
[63] Y. Liu, B. Derby, *Phys. Fluids* **2019**, *31*, 032004.
[64] A. Gao, J. Yan, Z. Wang, P. Liu, D. Wu, X. Tang, F. Fang, S. Ding, X. Li, J. Sun, M. Cao, L. Wang, L. Li, K. Wang, X. W. Sun, *Nanoscale* **2020**, *12*, 2569.
[65] C. Zheng, X. Zheng, C. Feng, S. Ju, Z. Xu, Y. Ye, T. Guo, F. Li, *Org. Electron.* **2021**, *93*, 106168.
[66] D. Hong, P. Zhao, Y. Du, C. Zhao, Y. Xia, Z. Wei, Z. Jin, Y. Tian, *iScience* **2020**, *23*, 101415.
[67] A. F. Gualdrón-Reyes, S. J. Yoon, E. M. Barea, S. Agouram, V. Muñoz-Sanjosé, Á. M. Meléndez, M. E. Niño-Gómez, I. Mora-Seró, *ACS Energy Lett.* **2018**, *4*, 54.